ACS Catalysis

Research Article

pubs.acs.org/acscatalysis

# Barium Substituted Lanthanum Manganite Perovskite for $CO_2$ Reforming of Methane

Annabathini Geetha Bhavani,[†] Won Yong Kim,[†] and Jae Sung Lee*[,‡]

[†]Department of Chemical Engineering, Pohang University of Science & Technology (POSTECH), Republic of Korea

[‡]School of Nano-Bioscience and Chemical Engineering, Ulsan National Institute of Science & Technology (UNIST), Republic of Korea

Supporting Information

**ABSTRACT:** Barium substituted lanthanum manganite $La_{1-x}Ba_xMnO_3$ ($x$ = 0.10−0.50) of a single phase perovskite structure was used as catalysts for $CO_2$ reforming of $CH_4$ for the first time. The optimal level of Ba substitution (Ba/Mn = 0.10, 0.15) produced $La_{1-x}Ba_xMnO_3$ of high surface area, uniform particle dispersion, and highly ordered pores. The optimally substituted perovskite catalysts showed much improved reducibility of $Mn^{3+}/Mn^{4+}$ to $Mn^{2+}$ to provide oxygen vacancies and rapid migration of lattice oxygen from the bulk toward the surface. The ability of donating lattice oxygen to the catalytic cycle seems responsible for the facilitated decomposition and dissociation of $CH_4$ and $CO_2$, which led to high conversions, excellent syngas selectivity, and stability with little coke formation. The addition of oxygen to the dry reforming reaction showed improved conversion and selectivity to syngas by making catalysts less prone to coke formation. To the best of our knowledge, the results represent the first example of Mn-based reforming catalysts that perform better than more common Ni-based catalysts of the same structure.

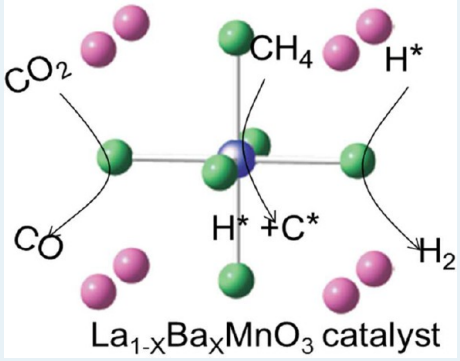


**KEYWORDS:** *$LaMnO_3$, Ba substitution, oxygen mobility, dry methane reforming, autothermal $CO_2$ reforming*

## 1. INTRODUCTION

Methane is the predominant component of natural gas that forms a major part of the energy market today. The combustion of natural gas and other fossil fuels to meet domestic, industrial, and automotive energy demands causes emission of $CO_2$. Methane and $CO_2$ are the two most important greenhouse gases contributing to global warming. Reforming of $CH_4$ with $CO_2$ converts them into syngas ($H_2$ + CO), which has a wide range of uses in synthetic chemistry. Thus, $CO_2$ reforming of $CH_4$ contributes not only to mitigation of the global environmental problem but also to the supply of a valuable chemical feedstock.

Methane reforming involves reactions of $CH_4$ with steam or another oxidant under high temperatures and pressures in the presence of metal catalysts that are prone to sintering and deactivation under harsh operating conditions. The formation of solid carbon ("coke") on the catalyst surface during the reaction is the most common cause of the catalyst deactivation by blocking reactant molecules from access to the active metal sites. Carbon deposition is attributed to two main reactions, i.e., direct $CH_4$ decomposition and the disproportionation of CO. It is favored on acidic supports such as $SiO_2$, while Lewis base supports have been reported to reduce carbon deposition.[1] Lewis bases have a high affinity for the chemisorption of $CO_2$ leaving oxygen on the catalyst surface, and the adsorbed oxygen reacts with deposited carbon to form CO, thereby retarding coke formation. The rate of catalytic reactions can be enhanced by the use of smaller metal crystallites in order to maximize the metal surface area. Therefore, the use of nanosized metal particles on basic supports is considered favorable for the reforming of $CH_4$ with $CO_2$.[2]

Perovskite-type mixed oxides ($ABO_3$), where A and B represent 12-coorbination and 6-coordination metal cations, respectively, are promising materials for catalytic applications involving high temperatures, because of their thermochemical stability and tunable catalytic performance. In general, the A position is occupied by lanthanide metals (La, Pr, Nd, Sm, etc.) or alkaline earth metals (Sr, Ca, Ba, etc.) and the B position by an element chosen from transition metals (Fe, Co, Ni, Mn, Cr, Cu, V, etc.). The catalytic activity of the perovskite can be tailored by partial substitution of A- and/or B-site cations, which can lead to structural defects by stabilization of unusual oxidation states by B components. The attractive attributes of perovskite oxides for catalytic applications include the high mobility of oxygen and stabilization of unusual cation oxidation states in this structure, together with the thermal stability at high temperatures.[3−5]

The $CO_2$ reforming of $CH_4$ requires high temperatures to secure thermodynamically favorable conditions, and it is natural that many researchers have tested perovskite oxides as catalysts for this reaction.[6] Under the highly reducing reaction conditions at the high temperatures, the perovskite oxides are

Received: March 30, 2013
Revised: May 15, 2013
Published: May 20, 2013

   dx.doi.org/10.1021/cs400245m | ACS Catal. 2013, 3, 1537−1544

Table 1. Surface Area and Elemental Composition of $La_{1-X}Ba_XMnO_3$ Perovskite Oxide Catalysts

| sample code | catalyst | ba ratio ($x$) | surface area $S_g$ ($m^2/g$) | average pore diameter (Å) | lattice parameter (Å) | relative elemental composition | | |
|---|---|---|---|---|---|---|---|---|
| | | | | | | La | Ba | Mn |
| LM | $LaMnO_3$ | 0.0 | 6.5 | 11.8 | 3.861 | 0.99 | 0.00 | 1.00 |
| LBM-10 | $La_{0.90}Ba_{0.10}MnO_3$ | 0.10 | 10.8 | 13.3 | 3.872 | 0.91 | 0.10 | 1.00 |
| LBM-15 | $La_{0.85}Ba_{0.15}MnO_3$ | 0.15 | 13.4 | 13.5 | 3.887 | 0.84 | 0.15 | 1.00 |
| LBM-30 | $La_{0.70}Ba_{0.30}MnO_3$ | 0.30 | 8.6 | 12.8 | 3.889 | 0.69 | 0.31 | 1.00 |
| LBM-50 | $La_{0.50}Ba_{0.50}MnO_3$ | 0.50 | 6.8 | 12.4 | 3.902 | 0.51 | 0.52 | 1.00 |

known to be partially reduced to form nanosized metal particles of B site elements, which are not only active for the reforming reaction but also resistant to carbon deposition.[7] Thus, perovskite-type $NdCoO_3$ formed the well dispersed Co particles to become a highly promising catalyst for carbon-free $CO_2$ reforming of $CH_4$ combined with steam reforming and partial oxidation of $CH_4$ to syngas.[8] The $LaFeO_3$ catalyst was relatively stable, and the substitution of a part of Fe with Ni resulted in an increase in the activity in partial oxidation of $CH_4$, in which Ni was reduced to form the highly dispersed metal particles without collapsing the $LaFeO_3$ perovskite structure.[9] The kinetic behavior of the $LaNiO_3$ perovskite catalyst in $CO_2$ reforming of $CH_4$ was investigated, which showed two kinds of active sites on the catalyst surface: metallic Ni for activating $CH_4$ and basic $La_2O_3$ for $CO_2$.[10]

In contrast, lanthanum manganite $LaMnO_3$ perovskite has not been directly applied to $CH_4$ reforming reactions. Manganese itself is not usually considered an active phase of the $CH_4$ reforming but rather plays a secondary role to promote the nickel-based reforming catalysts.[11] Thus, Mn assists Ni dispersion and improves the resistance of $Ni/Al_2O_3$ catalysts to deactivation in $CO_2$ reforming of $CH_4$.[12] Yet, there have been significant amounts of previous reports on the catalytic applications of $LaMnO_3$ for high temperature reactions including combustion,[6] methane oxidation,[13] alcohol dehydrogenation,[14] and the cathode reaction of solid oxide fuel cells.[15] In many cases, A and/or B atoms are partially substituted by different atoms to modulate electronic, structural, and therefore catalytic properties of $LaMnO_3$. By noting that the thermochemical stability and facile redox properties of partially substituted $LaMnO_3$ were the impetus behind the popularity of $LaMnO_3$-based catalysts for these reactions, we applied the materials for the first time to the $CO_2$ reforming of $CH_4$, for which these properties are equally beneficial.

Thus, in the present work, we prepared Ba-substituted lanthanum manganites ($La_{1-x}Ba_xMnO_3$) using the sol−gel process and applied them as catalysts for the dry $CO_2$ reforming of $CH_4$ (DRM) and autothermal $CO_2$ reforming (ATR) of $CH_4$. Since a Lewis base activates $CO_2$, it could be an attractive concept to incorporate a more basic Ba into the thermally stable $LaMnO_3$ structure. In more common $Ni/Al_2O_3$ catalysts, introduction of an optimal level of Ba was shown to improve the stability of syngas production by a dry reforming process.[16] Recently, barium has received more attention in soot oxidation over the $Ba/MnO_x-CeO_2$ catalyst[17] and Ba−K/$CeO_2$.[18] As mentioned, partial substitution of $La^{3+}$ in $LaMnO_3$ with $Ba^{2+}$ also produces $Mn^{4+}$ and/or oxygen vacancy for charge compensation.[19] This system provides an opportunity to study the effect of lattice oxygen on their catalytic performance. As a result, we have discovered that partial Ba-substitution into $LaMnO_3$ dramatically improves the catalytic activity and stability of $La_{1-x}Ba_xMnO_3$ for both DRM and ATR reactions by affecting mainly the reducibility of the catalysts and mobility of lattice oxygen. It also provides a simple way to tune the reactivity of perovskite oxides for $CO_2$ reforming reactions of $CH_4$.

## 2. EXPERIMENTAL SECTION

**2.1. Synthesis of Ba-Substituted $LaMnO_3$.** The stoichiometric amounts of $La(NO_3)_3{\cdot}4H_2O$, $Mn(NO_3)_2{\cdot}4H_2O$, and $Ba(NO_3)_2{\cdot}4H_2O$ were used as precursors. A molar composition of citric acid and total metal ions of 1:1.5 was adopted to obtain the perovskite oxides by a sol−gel method. These precursors undergo various forms of hydrolysis and polycondensation reactions. The formation of a metal oxide involves connecting the metal centers with oxo (M−O−M) or hydroxo (M−OH−M) bridges, therefore, generating metal-oxo or metal-hydroxo polymers in solution. Thus, the sol evolves toward the formation of a gel-like diphasic system containing both a liquid phase and a solid phase, whose morphology ranges from discrete particles to continuous polymer networks. The resulting gel was placed in the furnace at 600 °C for 5 h to form a primary powder, and then, it was thermally treated at 1250 °C for 5 h.

The detailed characterization procedures of perovskite materials have been described in the Supporting Information (SI). The characterization includes the following: BET surface areas and pore size distribution by $N_2$-sorption, elemental analyses by inductively coupled plasma spectroscopy (ICP), crystal structure analysis by powder X-ray diffraction (XRD), temperature-programmed reduction (TPR), temperature-programmed desorption (TPD) of $O_2$ and $CO_2$, X-ray photoelectron spectroscopy (XPS), high resolution scanning electron microscopy (HR-SEM), and thermogravimetric analysis (TGA).

**2.2. Catalytic Reforming Reactions.** Catalytic reactions DRM and ATR were carried out in a tubular fixed-bed flow reactor of 1/2 in. (inside diameter) at atmospheric pressure. Typically 100 mg of catalyst was loaded (bed length 5−7 mm), preheated at 500 °C for 30 min, and then activated in flowing $H_2$ at 770 °C for 1 h. The reactions were performed at atmospheric pressure at 800 °C. The reactant gases had an inlet mole ratio of $CH_4/CO_2$ = 1:0.8 for DRM and $CH_4/CO_2/O_2$ = 1:0.8:0.2 for ATR, which were fed into the reactor at a gas hourly space velocity (GHSV) of 243,000 $h^{-1}$, and the gas flow rate was controlled by mass flow meters. To determine conversion and selectivity, the products were analyzed after 30 min of steady-state operation by an online gas chromatograph (Agilent Technologies 7890A, 60/80 Carboxen 1000 column) with a TCD detector. The conversions of $CH_4$ and $CO_2$ were calculated from the consumed reactants, and the selectivity of $H_2$ and CO was determined from their concentrations as defined previously.[11]


dx.doi.org/10.1021/cs400245m | ACS Catal. 2013, 3, 1537−1544

## 3. RESULTS AND DISCUSSION

**3.1. Physical Properties of Ba-Substituted $LaMnO_3$ Catalysts.** Pristine and Ba-substituted $LaMnO_3$ catalysts are denoted as LM and LBM-*x*, where *x* is the atomic fraction of Ba relative to La as shown in Table 1. The BET surface areas ($S_g$) of the perovskite catalysts obtained from $N_2$ adsorption clearly indicate a noticeable dependence on the degree of Ba substitution. They show significant increases for $x$ = 0.10 and 0.15, then further Ba substitution decreases $S_g$ progressively to the level of LM for LBM-50. The $S_g$ of LBM-15 catalyst was about twice as large as that of pristine LM. This trend of $S_g$ is consistent with that of average pore diameter although the variation is not as large. The elemental compositions of perovskite materials shown in Table 1 match well with those of the initial sol prepared.

The powder XRD patterns of the calcinied $La_{1-x}Ba_xMnO_3$ are exhibited in Figure 1, which shows a single perovskite phase

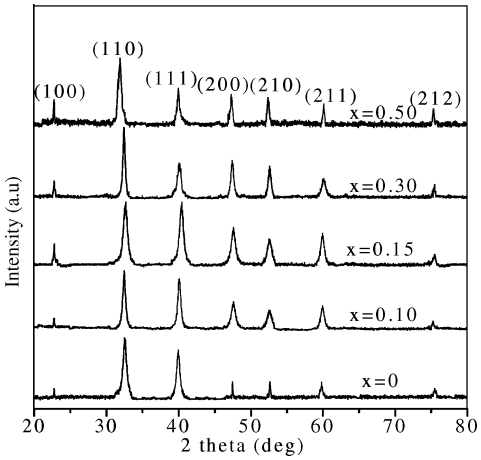


**Figure 1.** XRD patterns of $La_{1-x}Ba_xMnO_3$ perovskite oxide catalysts.

for all samples that could be indexed in a cubic symmetry. No impurity phase was found such as $BaMnO_3$ or $Ba_3Mn_2O_8$. Furthermore, XRD analysis also shows that the increasing Ba content leads to lattice enlargement (see lattice parameters in Table 1) all the way up to $x$ = 0.50, which could in turn accompany the progressive structural distortion. With increased Ba substitution, the crystallinity of the perovskite structure is lowered, and the main reflection of the (110) plane is slightly shifted toward lower angle. This is expected when larger $Ba^{2+}$ (radii 0.135 nm) replaces smaller $La^{3+}$ (0.106 nm) in the cubic perovskite structure, which leads to increased volume of the unit cell.[18] XRD patterns of reduced $La_{1-x}Ba_xMnO_3$ perovskite shown in Figure S1 (SI) indicate that all the catalysts retain their perovskite phase after reduction with only slightly decreased intensity. A small peak of $La_2O_3$ is noticed in all samples, indicating only a partial disruption of the original perovskite structure. Unlike perovskites containing Ni or Co,[7,9] there was no sign of metallic $Mn^0$ formation after reduction at 770 °C in hydrogen.

Figure 2 shows HR-SEM microstructures of $La_{1-x}Ba_xMnO_3$ reduced in an equimolar $H_2/N_2$ flow at 770 °C for 1 h. The LM specimen shows agglomerated particles of about 400 nm in diameter. In LBM-10, particles become smaller, porous, and roughly spherical and are distributed well, with particle sizes of ca. 270 nm. A further increase in Ba substitution ($x$ = 0.15) develops better ordered, porous microstructures with further

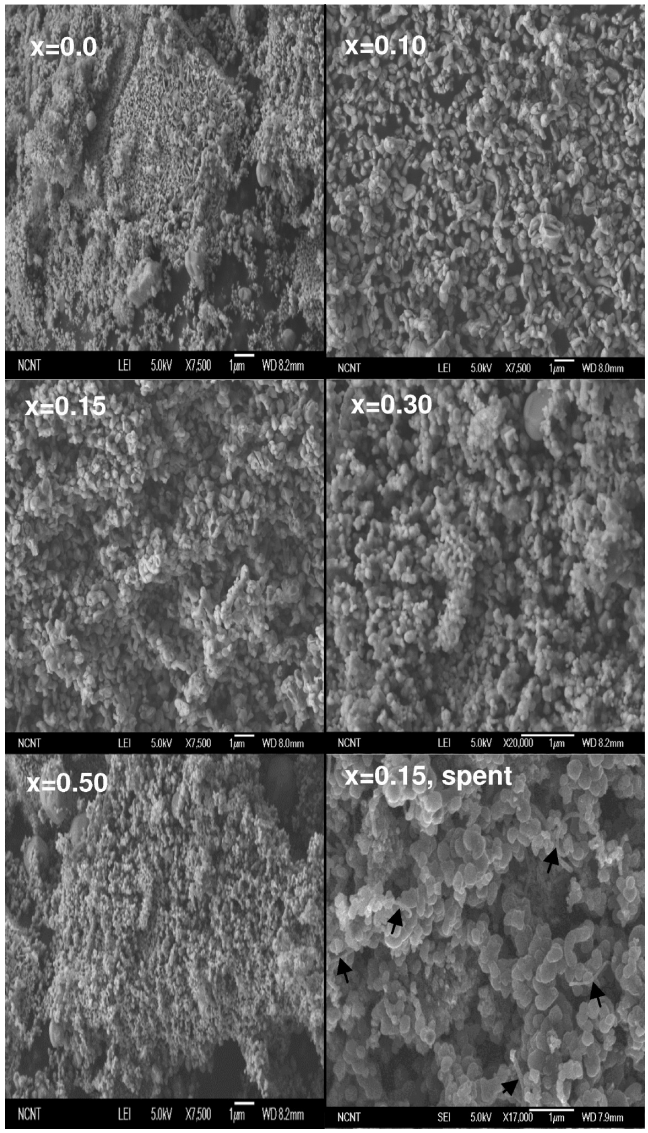


**Figure 2.** HR-SEM microstructural analysis of $La_{1-x}Ba_xMnO_3$ with different degrees of Ba substitution ($x$). The last image is for a spent catalyst in the ATR reaction at 800 °C for 24 h that shows a few carbon filaments as indicated.

reduced sizes of ca. 200 nm. Further higher Ba substitution increases the particle size and agglomeration that clearly decreases the porosity. This evolution of morphology is consistent with the trend of the change in $S_g$ in Table 1. The last image in Figure 2 is for spent $La_{1-x}Ba_xMnO_3$ ($x$ = 0.15) used in the DRM reaction at 800 °C for 24 h. The particles grew to ~400 nm during the reaction, but they did not show any serious agglomeration. A few filamentous carbons are seen as indicated that were formed during the reaction.

**3.2. Redox Properties of Ba-Substituted $LaMnO_3$ Catalysts.** Perovskites may exhibit structural defects due to deficiencies of cations at A or B sites or of oxygen anions.[20] The oxygen vacancies are more common and affect directly the catalytic properties of the material. The literature reports that the higher reducibility and oxygen storage/release capacity of perovskite oxide catalysts may promote the mechanism of continuous removal of carbonaceous deposits from active sites in reactions like partial oxidation and $CO_2$ reforming of $CH_4$.[21,22]


dx.doi.org/10.1021/cs400245m | ACS Catal. 2013, 3, 1537−1544

When a part of trivalent $La^{3+}$ ions of the parent $LaMnO_3$ are replaced by divalent $Ba^{2+}$, a part of the $Mn^{3+}$ ions are driven into the +4 state to preserve charge neutrality as shown in the following reaction:

$$La^{3+}Mn^{3+}O_3^{2-} \rightarrow La_{1-x}^{3+}Ba_x^{2+}Mn_{1-x}^{3+}Mn_x^{4+}O_3^{2-} \quad (1)$$

The formed species can be further transformed to form defects or oxygen vacancies depending on the temperature, oxygen partial pressure, and the value of $x$. There is an exchange of electrons from neighboring $Mn^{3+}$ to $Mn^{4+}$ ions, which is responsible for the creation of oxygen vacancies.

$$La_{1-x}^{3+}Ba_x^{2+}Mn_{1-x}^{3+}Mn_x^{4+}O_3^{2-} \rightarrow La_{1-x}^{3+}Ba_x^{2+}Mn_{1-x+2\delta}^{3+}Mn_{x-2\delta}^{4+}O_{3-\delta}^{2-} + \delta/2O_2 \quad (2)$$

Thus, Ba-substitution affects the behavior of the lattice oxygen and the redox properties of perovskite oxides and eventually dictates their catalytic properties. In order to study the redox properties of $La_{1-x}Ba_xMnO_3$, we employed temperature-programmed reduction (TPR) by $H_2$ and temperature-programmed desorption (TPD) of $O_2$.

The $H_2$-TPR profile represents the reducibility of the oxide catalysts, which is associated with its ability to liberate oxygen from the catalyst by reaction with $H_2$. As can be seen from Figure 3, all the catalysts show two reduction peaks of the active component, and their peak temperature and intensity depend on the degree of Ba-substitution in $La_{1-x}Ba_xMnO_3$. The Ba-substituted perovskite catalysts show reduction peaks shifted toward lower temperatures compared to the pristine $LaMnO_3$. The first reduction peak at 350−450 °C is assigned to the removal of the chemisorbed surface oxygen and the reduction of $Mn^{4+}$ formed to compensate for the cation vacancy caused by $Ba^{2+}$ ion incorporation. The intensity of this peak increases with $x$. The second reduction peak at 610−880 °C behaves similarly to the low temperature peak and is attributed to reduction of $Mn^{3+}$ to $Mn^{2+}$.[23] Thus, it represents oxygen released from the bulk of the solid. The total hydrogen consumption of the perovskite materials is shown in Table 2.

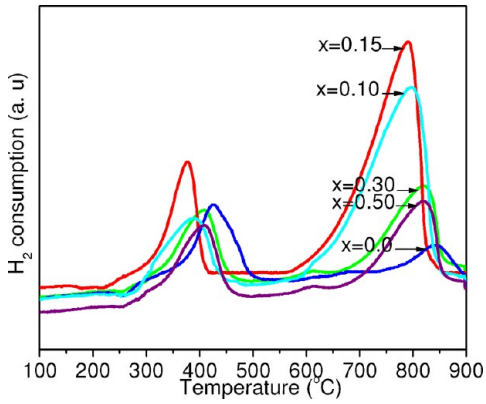


**Figure 3.** $H_2$-TPR profiles of $La_{1-X}Ba_XMnO_3$ perovskite oxide catalysts.

The $LaMnO_3$ catalyst shows the lowest hydrogen consumption, which increases with Ba-substitution to the maximum value for LBM-15 and then decreases with further substitution. Since the reforming reactions take place at 800 °C in the presence of $H_2$ and CO, the amount of hydrogen consumption represents the amount of oxygen that the catalyst can provide to the reaction. Figure 3 also shows that Ba-substitution shifts the second reduction peak from 820 °C to a lower temperature of 740 °C, and the peak is broadened. This represents a rapid migration of lattice oxygen from the bulk toward the surface in the Ba-substituted catalysts. The results of $H_2$-TPR clearly indicate that Ba-substitution improves the reducibility of $Mn^{n+}$ in $LaMnO_3$ both kinetically (lower temperatures) and in degree of reduction (larger amounts).

For oxygen TPD, the reduced sample was treated in an $O_2$/Ar flow (30 mL/min) from 30 to 900 °C and then lowered to room temperature and evacuated for 30 min. The $O_2$ desorption was monitored by mass spectrometer in a He flow while heating from 30 to 900 °C at a rate of 10 °C/min. The oxygen TPD spectra ($m/z$ = 32 amu) in Figure 4 show two desorption peaks at low and high temperatures. The total amounts of $O_2$ desorption estimated from the integration of these peaks are listed in Table 2. The low temperature peak at 200−350 °C is ascribed to the adsorbed oxygen, whereas the high temperature desorption peak at 600−850 °C is attributed

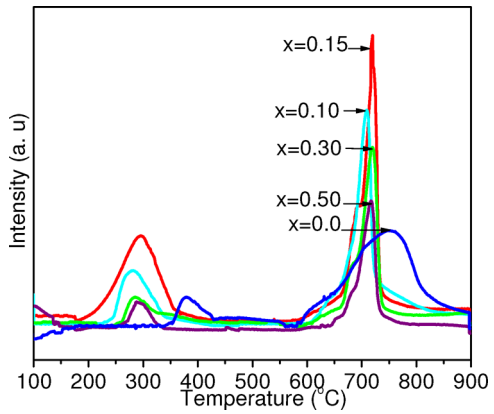


**Figure 4.** $O_2$-TPD profiles of $La_{1-X}Ba_XMnO_3$ perovskite oxide catalysts.

**Table 2. Chemisorption, XPS, and Coke Formation Properties of $La_{1-X}Ba_XMnO_3$ Perovskite Catalysts**

| sample code | $H_2$ consumption ($\mu$ mol/g)[a] | $O_2$ desorption ($\mu$ mol/g)[a] | $CO_2$ desorption ($\mu$ mol/g)[a] | content of $Mn^{4+}$ %[b] | coke content DRM wt %[c] | coke content ATR wt %[c] |
|---|---|---|---|---|---|---|
| LM | 156.3 | 86.0 | 21.7 | 12.4 | 24.6 | 17.4 |
| LBM-10 | 374.1 | 204.1 | 78.9 | 63.7 | 5.1 | 2.3 |
| LBM-15 | 456.8 | 229.9 | 94.7 | 84.4 | 2.9 | 1.1 |
| LBM-30 | 342.2 | 108.4 | 61.5 | 46.8 | 9.4 | 4.6 |
| LBM-50 | 227.9 | 98.3 | 56.4 | 42.0 | 19.5 | 6.7 |

[a]Measured from $H_2$-TPR, $O_2$-TPD, and $CO_2$-TPD experiments. [b]Determined from Gaussian fitting of XPS spectra. [c]Measured by TGA of spent catalysts after 24 h of on stream reactions. ATR, autothermal $CO_2$ reforming with methane; DRM, dry reforming.


dx.doi.org/10.1021/cs400245m | ACS Catal. 2013, 3, 1537−1544

to the lattice oxygen ($O^{2-}$) in general.[24] The lattice oxygen originates from the reduction process involving the B-site cation ($Mn^{n+}$) and leads to the formation of oxygen vacancies. Introduction of $Ba^{2+}$ ions on the $La^{3+}$ site also creates oxygen vacancies within the perovskite structure.[6] The changes in intensity of the two peaks with an $x$ ratio in LBM perovskites have been interpreted in terms of the change in the electronic configuration including the increased $Mn^{4+}$ content, which lowers the binding energy of oxygen in Mn−O.[25]

It is clear from Table 2 that Ba addition to the perovskite structure significantly improves the adsorbed and lattice oxygen from 86 $\mu$mol (LM) to 229.9 $\mu$mol (LBM-15), but it gradually decreases upon further increasing the Ba loading ($x$ = 0.30, $x$ = 0.50). We assume that decreased desorption may be due to the excess substituent with larger ionic radii ($Ba^{2+}$), which may partially cover the $Mn^{n+}$ and make it difficult to reduce. This may be related to the formation of the larger crystals as is evident in the FE-HRSEM of Figure 2 ($x$ = 0.30 and $x$ = 0.50). This trend is in general agreement with the results of $H_2$-TPR and indicates that an appropriate amount of Ba-substitution into the $LaMnO_3$ lattice improves the capacity of oxygen that could be released from the catalyst during the reforming reactions. Thus, both $H_2$-TPR and $O_2$-TPD provide a consistent picture on the behavior of the lattice oxygen and the redox properties of perovskite oxides. The Ba-substituted perovskite catalysts showed much improved ability of donating lattice oxygen to provide oxygen vacancies with rapid migration of lattice oxygen from the bulk toward the surface.

**3.3. Photoelectron Spectroscopy (XPS).** The electronic states of $La_{1-x}Ba_xMnO_3$ perovskite were monitored by XPS analysis of O 1s and Mn 2p peaks. The O 1s binding energy region reveals two distinctive XPS peaks in Figure S2 in the SI. The peak at low binding energy (BE 530.0 eV) is assigned to lattice oxygen $O^{2-}$ ($O_{lattice}$), and the high binding energy (BE 531.4 eV) peak is assigned to adsorbed oxygen species ($O_{adsorbed}$). Liu et al.[26] noticed a clear influence of $x$ on the XPS spectra of the lattice oxygen and absorbed oxygen species in $Sm_{2-2x}Sr_{1+2x}Mn_2O_7$ perovskite. In the present case, increasing Ba substitution from 0.0 to 0.15 efficiently increases the intensity of both lattice oxygen and adsorbed oxygen species, but a further increase to 0.30 and 0.50 decreases the intensity of the two peaks. This evolution of oxygen signal may represent the different degrees of oxygen close to the surface due to their different surface areas.

Manganese in $LaMnO_3$ is formally trivalent $Mn^{3+}$, and its Mn 2p XPS peak exhibits a dominant $Mn^{3+}$ signal. Since La is a trivalent ion and Ba is divalent, chemical substitution of La ions by Ba ions leads to the change in Mn ion valence, as already mentioned, to a mixture of $Mn^{4+}$ and $Mn^{3+}$ ions in $La_{1-x}Ba_xMnO_3$.[27] Valence conversion of Mn in this material can provide concrete information on the distribution of Ba in the A site, possibly leading to a better understanding of its catalytic property. Figure 5 shows XPS spectra of Mn 2p core levels ($2p_{3/2}$, $2p_{1/2}$) for LM and LBM perovskites. The $2p_{3/2}$ peaks are located close to 642.4 eV for $Mn^{4+}$ and 641.3 eV for $Mn^{3+}$ ions and $2p_{1/2}$ at 654.2 eV. Pristine LM perovskite shows a dominant $Mn^{3+}$ phase, but the $Mn^{4+}$ phase grows with $Ba^{2+}$ substitution for LBM-10 and LBM-15 perovskites and then decreases again upon further Ba substitution. This trend could be confirmed in the fractions of $Mn^{4+}$ (the rest is $Mn^{3+}$) in Table 2 obtained from the peak deconvolution with Gaussian fitting of the experimentally obtained spectra. The maximum $Mn^{4+}$ ion content is observed at $x$ = 0.15. These data explicitly

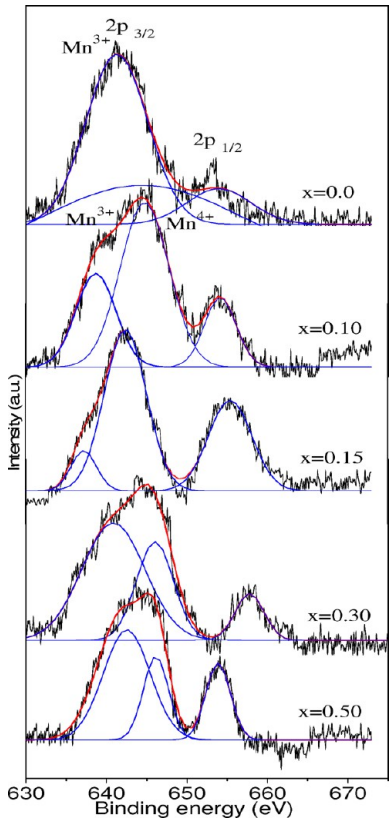


**Figure 5.** XPS analysis for $La_{1-X}Ba_XMnO_3$ samples, Mn 2p core level spectra.

illustrate the evolution of mixed valence states of the $Mn^{n+}$ ions with respect to the degree of Ba substitution ($x$).

**3.4. Basicity of the Catalysts.** The basic property of the catalysts plays a key role in adsorption and dissociation of $CO_2$ to produce CO. The basicity of the perovskite materials is investigated with the TPD of $CO_2$, which is a popular acidic probe molecule as well as a reactant of the reforming reactions. Figure 6 indicates the temperature range wherein $CO_2$ chemisorbed on the basic sites is desorbed, and the total amount of desorbed $CO_2$ is listed in Table 2. All the catalysts show two desorption peaks with varying intensities around ~300 °C and ~750 °C representing relatively weak and strong basic sites, respectively. The addition of Ba to LM catalyst

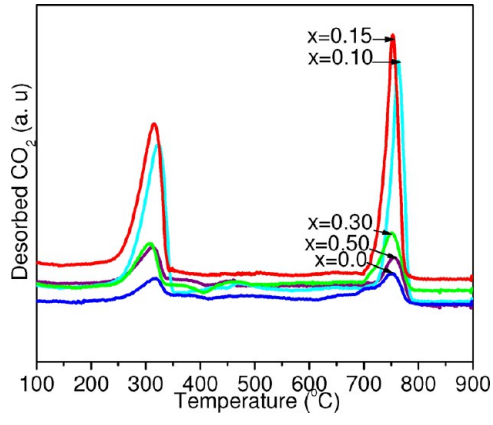


**Figure 6.** $CO_2$ desorption profiles of $La_{1-X}Ba_XMnO_3$ perovskite oxide catalysts.


dx.doi.org/10.1021/cs400245m | ACS Catal. 2013, 3, 1537−1544

increases the intensity of both low and high temperature peaks. The position of the low temperature peaks increases with the addition of $Ba^{2+}$, indicating that Ba addition increases the number of basic sites as well as their strength. The intense desorption peak at ~750 °C indicates very strong basic sites, which may be due to the decomposition of alkali carbonates.

The total amount of $CO_2$ desorption also shows the maximum for LBM-15 catalyst, and its desorption peak shifts to a slightly lower temperature of ~740 °C. In a different system, Hong et al.[28] reported that the highest NO decomposition activity was achieved over a Ba/CeMn mixed oxide catalyst that showed the maximum basicity with an optimal Ba loading, and the higher Ba loading decreased the basicity due to decreased dispersion of Ba species on the catalyst surface. Thus, the high basicity of LBM-10 and LBM-15 may originate from their large amounts of exposed Ba due to their high surface areas.

**3.5. Dry $CO_2$ Reforming of $CH_4$.** The LM and LBM catalyst series were tested for DRM reaction after reduction in an equimolar $H_2/N_2$ flow at 770 °C for 1 h. The dry reforming reaction is represented as follows:

$$CH_4 + CO_2 \rightarrow 2H_2 + 2CO \ (\Delta H^\circ = 264\ \text{kJ/mol}) \quad (3)$$

The catalytic activity tests were performed at 800 °C with a mole ratio of $CH_4/CO_2$ = 1:0.8 over reduced perovskite catalysts, and conversions of $CH_4$ and $CO_2$ and selectivity to CO and $H_2$ are exhibited in Figure 7. The amounts of coke formed over the catalysts were determined as listed in Table 2 by TGA analysis after 24 h of on-stream reaction.

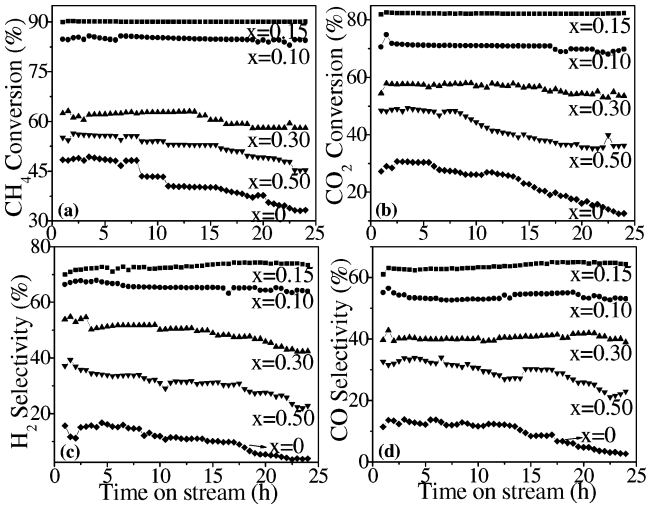


**Figure 7.** Catalytic activity for dry reforming of methane with $CO_2$ over $La_{1-X}Ba_XMnO_3$ perovskite oxide catalysts: (a) $CH_4$ conversion, (b) $CO_2$ conversion, (c) $H_2$ selectivity, and (d) CO selectivity.

The LM catalyst shows low and unstable reforming activity: $CH_4$ conversion decreases from an initial 48.4% to a final 33.3%, and $CO_2$ conversion drops from an initial 27.3% to a final 12.5%. During 24 h of on-stream reaction, the LM catalyst shows the largest amount of carbon deposition of 24.6 wt %. The Ba substitution into the LM catalyst shows a remarkable increase in activity as well as stability up to LBM-15. It shows the best activity with $CH_4$ conversion of ca. 90% and $CO_2$ conversion of ca. 82%. These conversions remain almost invariant for 24 h, which is consistent with the greatly reduced carbon formation of 2.9 wt %. Prolific formation of carbon fibres on LM catalysts and dramatically reduced carbon formation are nicely demonstrated by FE-SEM images in Figure S3 in the SI. A further increase in Ba substitution in LBM-50 shows a decrease in activity and stability together with increasing coke formation. Selectivities for $H_2$ are generally higher than those of CO. The LM catalyst shows unstable and low selectivities of 15.8% for $H_2$ and 11.5% for CO. Both $H_2$ and CO selectivities increased with Ba substitution and reached a maximum over the LBM-15 catalyst with 70% and 61%, respectively. A further increase in Ba substitution decreases the syngas production. The performance of Ba-substituted $LaMnO_3$ catalysts was in general superior to the more common $LaNiO_3$-based catalysts. Thus, Moradi et al.[29] studied the dry reforming of methane with $LaNiO_3$ and $La_{0.9}Ba_{0.1}NiO_3$ perovskite catalysts, where $CH_4$ conversion increased from 45% to 55% and $CO_2$ from 39% to 51% with the addition of Ba. Thus, LBM series catalysts are the rare example that Mn-based catalysts with $Mn^{n+}$ as an active catalytic species perform better than more common Ni-based catalysts for dry methane reforming in conversions as well as stability with negligible amounts of coke formation.

The instability in conversions and selectivity is correlated well with the amounts of carbon deposition. Carbon deposition can be attributed to two main reactions, direct methane decomposition and the disproportionation of carbon monoxide.

Methane decomposition:

$$CH_4 \rightarrow C + 2H_2 \quad \Delta H^\circ = 75\ \text{kJ mol}^{-1} \quad (4)$$

Boudouard reaction:

$$2CO \rightarrow C + CO_2 \quad \Delta H^\circ = -171\ \text{kJ mol}^{-1} \quad (5)$$

The formation of solid carbon ultimately forms a barrier on the surface of the catalyst that prevents reactant molecules from accessing the active sites, leading to deactivation. The other side reaction to consider is the reverse water−gas shift reaction which consumes $H_2$ and $CO_2$ to produce additional CO, thereby leading to higher conversions of $CO_2$ than $CH_4$.

Reverse water−gas shift:

$$CO_2 + H_2 \rightarrow CO + 2H_2O \quad (6)$$

**3.6. Autothermal $CO_2$ Reforming of Methane.** The ATR reaction uses oxygen and carbon dioxide in a reaction with methane to form syngas. The reaction takes place in a single chamber where the methane is partially oxidized in an exothermic reaction and carbon dioxide is reduced in an endothermic reaction. The combination of exothermic and endothermic reactions is a very important accomplishment to obtain temperature compensation of the process. The reactions can be described in the following equation:

$$2CH_4 + O_2 + CO_2 \rightarrow 3H_2 + 3CO + H_2O \quad (7)$$

The catalytic performances obtained for reduced $La_{1-x}Ba_xMnO_3$ with different Ba ratios are compared for the ATR reaction in Figure 8, where conversions of $CH_4$ and $CO_2$ and selectivities to $H_2$ and CO are plotted against time on stream at 800 °C and with a reactant mole ratio of $CH_4/CO_2/O_2$ = 1:0.8:0.2. The relative activities among different perovskite catalysts are the same as those for the DRM reaction except for both $CH_4$ and $CO_2$ conversions in ATR for all catalysts with different degrees of Ba substitution. The LM catalyst shows initially $CH_4$ and $CO_2$ conversions of 79.8% and 47.3% that drop to 65.2% and 37.4% with 17.4 wt % of carbon


dx.doi.org/10.1021/cs400245m | ACS Catal. 2013, 3, 1537−1544

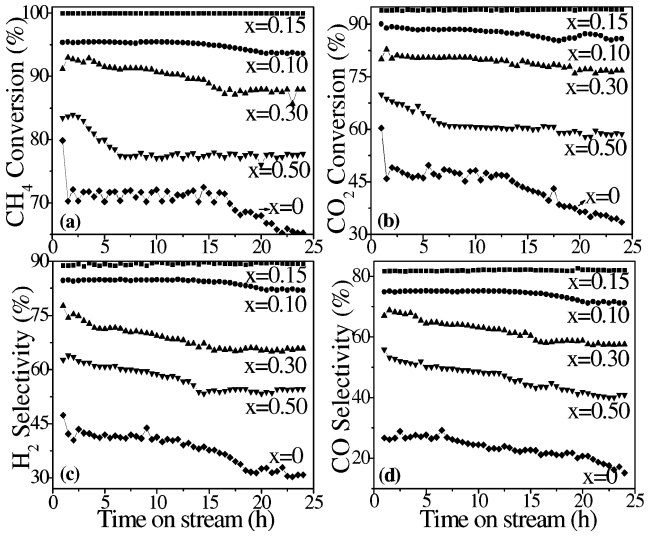


**Figure 8.** Catalytic activity of autothermal $CO_2$ reforming of methane over $La_{1-X}Ba_XMnO_3$ perovskite oxide catalysts: (a) $CH_4$ conversion, (b) $CO_2$ conversion, (c) $H_2$ selectivity and (d) CO selectivity.

deposition in 25 h on stream. Ba-substituted LBM series catalysts show remarkable improvement in catalytic activity of initial $CH_4$ and $CO_2$ conversions and their maintenance. For the best case, the LBM-15 catalyst shows initially 100% and 94% of $CH_4$ and $CO_2$ conversions that are maintained for 24 h without a noticeable deactivation. Carbon deposition during this period is a meager 1.1 wt %. This catalyst also shows the highest $H_2$ and CO selectivities of 81.7% and 88.9%, which remain stable during the whole time on stream. Interestingly, ATR reaction shows less coke formation than the DRM reaction as confirmed by TGA in Table 2. Oxygen addition to the DRM reaction increases conversions and reduces carbon deposition on the catalyst surface probably by instigating the activation of reactants and oxidation of coke. The FE-HRSEM images of LBM-15 and LM catalysts in Figure S3 in the SI show much reduced coke formation in the ATR reaction than in the DRM reaction in line with the results of TGA analysis in Table 2.

**3.7. Effects of Lattice Oxygen in DRM and ATR.** The Ba substitution into the $LaMnO_3$ perovskite lattice exerts profound effects as discussed above in both ATR and DRM reactions. Remarkable improvement and stable maintenance of $CH_4/CO_2$ conversions and selectivities to $H_2/CO$ are observed when an appropriate amount of Ba ($x$ = 0.10, 0.15) substitutes La in A sites of the perovskite structure. It is well-known that Ba-substitution brings the change in electronic structure of $LaMnO_3$, i.e., the change in manganese ion valence from $Mn^{3+}$ to a mixture of $Mn^{4+}$ and $Mn^{3+}$ ions in $La_{1-x}Ba_xMnO_3$ to compensate for the charge imbalance when a divalent $Ba^{2+}$ ion replaces a trivalent $La^{3+}$ ion in the perovskite structure. It modifies several properties of $LaMnO_3$ including increased surface area, uniform pore structure, and increased surface basic sites. These modified properties are all favorable for the high activity and stability of $CO_2$ reforming of $CH_4$. But the most important determining factor in the catalytic activity caused by the Ba substitution appears to be the dramatically improved reducibility of $Mn^{3+}/Mn^{4+}$. As probed by $H_2$-TPR and $O_2$-TPD, more lattice oxygen is released at a faster rate from LBM series catalysts compared to the unmodified LM catalyst. The morphological changes may also contribute to the improved reducibility, i.e. oxygen diffusion from bulk to surface by smaller particle sizes (by FE-HRSEM images) and easier accessibility by the reactants due to enlarged pores. This oxygen mobility improves significantly the activation and oxidation of the carbon formed.

It is generally accepted that the initial step of methane reforming occurs over a reduced metallic site by decomposition, whereas $CO_2$ dissociation occurs over lattice oxygen adjacent to the site, as shown in Figure 9. Thus, chemisorption

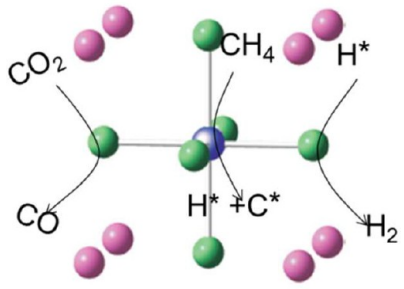


**Figure 9.** Sequence of elementary steps for $CH_4$ decomposition, $CO_2$ dissociation, and water gas shift reactions over $La_{1-X}Ba_XMnO_3$ perovskite oxide. Blue, Mn; green, O; and red, La/Ba. The activation of methane to C* involves reduced $Mn^{n+}$, whereas $CO_2$ dissociation to CO occurs over a vacant lattice oxygen site adjacent to the $Mn^{n+}$ site.

and the breaking of C−H bonds of methane involve reduced $Mn^{n+}$.

$$CH_4 \rightarrow CH_3^* \rightarrow CH_2^* \rightarrow CH^* \rightarrow C^* \quad (8)$$

Hydrogen is liberated as a gaseous hydrogen product. If elemental carbon is exposed to the reaction conditions long enough, it tends to be polymerized to form coke. But if the oxygen atom is supplied in time, the carbon could be removed as CO before polymerization.[30]

$$C^* + O^* \rightarrow CO + 2^* \quad (9)$$

The efficiency of this step is essential for the catalysts to have high activity and stability with minimal coke formation in methane reforming reactions. The sources of oxygen could be oxygen-containing reactants and intermediates such as $CO_2$, $H_2O$, and in the case of ATR, $O_2$.

$$CO_2 + * \rightleftarrows CO + O^* \quad (10)$$

$$H_2O + * \rightleftarrows H_2 + O^* \quad (11)$$

$$O_2 + 2^* \rightleftarrows 2O^* \quad (12)$$

Since all these steps require the activation of a gaseous molecule by the catalyst, it would be easier to use surface and bulk oxygen contained in the catalyst.[27,31,32] In $H_2$-TPR and $O_2$-TPD, it was shown that these oxygen species are easily available at the reaction conditions. In particular, Ba-substituted $La_{1-x}Ba_xMnO_3$ ($x$ = 0.10, 0.15) perovskite catalysts are especially efficient to donate surface and lattice oxygen to accelerate the catalytic cycle. This feature plays a vital role for DRM and ATR reactions to maintain high and stable activity. It has been reported that the amount and the mobility of the oxygen species play key role in coke gasification. Xiaoping et al.[31] synthesized the $LaFeO_3$ perovskite catalyst and used it as an oxygen donor for partial oxidation of methane for synthesis gas production. Thus for LBM-10 and LBM-15 catalysts, the amount of lattice oxygen and rate of oxygen migration from the


dx.doi.org/10.1021/cs400245m | ACS Catal. 2013, 3, 1537−1544

bulk to the surface are the highest to yield the best performance of reforming reactions.

Now the used oxygen species has to be replenished by reactant molecules, and in particular, activation of $CO_2$ would be a critical step in $CO_2$ reforming reactions to sustain the turnover of the catalytic cycle. The Ba-introduction in the $LaMnO_3$ catalyst was found to increase the density of the basic sites, which provides the sites for $CO_2$ adsorption.[33,34] Also, the reduced surfaces are represented by metal−oxygen vacancy, and Ba-substitution creates oxygen vacancies according to reaction 2. Thus with an optimal combination of high oxygen vacancies and basicity induced by Ba substitution, this $CO_2$ reduction part of the catalytic cycle is also accelerated. This oxygen replenishing step becomes much more facile when $O_2$ is present in the gas phase in ATR reactions, giving higher conversions and less carbon deposition. The $CH_4/CO_2$ conversions, $H_2/CO$ selectivities, and stability decrease for excessive Ba content (LBM-30, LBM-50 catalysts). This is strongly correlated with the trend of the reducibility or redox properties with $Ba^{2+}$ content. This trend is also consistent with the variation of textural properties, i.e., surface area, uniformity in particles dispersion and pore sizes.

## 4. CONCLUSION

Barium was successfully substituted in the A site of $LaMnO_3$ by replacing $La^{3+}$ using a sol−gel process to develop the single phase perovskite $La_{1-x}Ba_xMnO_3$ with good chemical homogeneity. The optimal level of Ba substitution leads to $La_{1-x}Ba_xMnO_3$ of high surface area, uniformity in particle dispersion, and highly ordered pores. This optimized substituted perovskite catalyst showed much improved reducibility of $Mn^{n+}$ to provide oxygen vacancies and rapid migration of lattice oxygen from the bulk toward the surface. In DRM and ATR reactions, these catalysts showed high $CH_4$ and $CO_2$ conversions, excellent syngas selectivity, and robust maintenance of these performances with little coke formation, which were better than more common Ni-based catalysts of the same structure. The ability of donating lattice oxygen to the catalytic cycle seems responsible for the lofty performance of optimized $La_{1-x}Ba_xMnO_3$ catalysts. The addition of gaseous oxygen in the ATR reaction made the catalysts more active, and less prone to coke formation than the DRM reaction.

## ■ ASSOCIATED CONTENT

### Supporting Information

Additional information as mentioned in the text. This material is available free of charge via the Internet at http://pubs.acs.org

## ■ AUTHOR INFORMATION

### Corresponding Author

*Fax: +82-52-217-1019. E-mail: jlee1234@unist.ac.kr.

### Notes

The authors declare no competing financial interest.

## ■ ACKNOWLEDGMENTS

We gratefully acknowledge the financial support from POSCO and Basic Science Research Program (No. 2012-017247) of NRF Korea.

## ■ REFERENCES

(1) Ferreira-Aparicio, P.; Rodríguez-Ramos, I.; Anderson, J. A.; Guerrero-Ruiz, A. *Appl. Catal., A* **2000**, *202* (2), 183−196.
(2) Hu, Y. H. *Catal. Today* **2009**, *148* (3−4), 206−211.
(3) Royer, S.; Alamdari, H.; Duprez, D.; Kaliaguine, S. *Appl. Catal., B* **2005**, *58*, 273−288.
(4) Jimenez, V. M.; Fernandez, A.; Espinos, J. P.; Gonzalez-Elipe, A. R. *J. Electron Spectrosc. Relat. Phenom.* **1995**, *71*, 61−71.
(5) Jimenez, V. M.; Espinos, J. P.; Gonzalez-Elipe, A. R. *Surf. Interface Anal.* **1998**, *26*, 62−71.
(6) Ponce, S.; Peña, M. A.; Fierro, J. L. G. *Appl. Catal., B* **2000**, *24*, 193−205.
(7) Choudhary, V. R.; Uphade, B. S.; Balhekar, A. A. *J. Catal.* **1996**, *163*, 312−318.
(8) Choudhary, V. R.; Mondal, K. C. *Appl. Energy* **2006**, *83*, 1024−1032.
(9) Provendier, H.; Petit, C.; Estournes, C.; Libs, S.; Kiennemann, A. *Appl. Catal., A* **1999**, *180*, 163−173.
(10) Moradi, G. R.; Rahmanzadeh, M.; Sharifnia, S. *Chem. Eng. J.* **2010**, *162*, 787−791.
(11) Bhavani, A. G.; Kim, W. Y.; Kim, J. Y.; Lee, J. S. *Appl. Catal., A* **2013**, *450*, 63−72.
(12) Seok, S. H.; Choi, S. H.; Park, E. D.; Han, S. H.; Lee, J. S. *J. Catal.* **2002**, *209*, 6−15.
(13) Hammami, R.; Aïssa, S. B.; Batis, H. *Appl. Catal., A* **2009**, *353*, 145−153.
(14) Klimkiewicz, R.; Trawczyński, J. *Appl. Catal., A* **2009**, *360*, 199−204.
(15) Yang, J.; Muroyama, H.; Matsui, T.; Eguchi, K. *J. Power Sources* **2012**, *204*, 25−33.
(16) García-Diéguez, M.; Herrera, M. C.; Pieta, I. S.; Larrubia, M. A.; Alemany, L. J. *Catal. Commun.* **2010**, *11*, 1133−1136.
(17) Wu, X.; Liu, S.; Lin, F.; Weng, D. *J. Hazard. Mater.* **2010**, *181*, 722−728.
(18) Peralta, M. A.; Milt, V. G.; Cornaglia, L. M.; Querini, C. A. *J. Catal.* **2006**, *242*, 118−130.
(19) Slobodin, B. V.; Surat, L. L.; Vladimirova, E. V. *J. Alloys Compd.* **2002**, *335* (1−2), 115−119.
(20) Peña, M. A.; Fierro, J. L. G. *Chem. Rev.* **2001**, *101*, 1981−2017.
(21) Valderrama, M. R.; Goldwasser, C. U.; De Navarro, J. M.; Tatiboue, J.; Barrault, C.; Batiot-Dupeyrat, F. M. *Catal. Today* **2005**, *107*, 785−791.
(22) de Lima, S. M.; da Silva, A. M.; da Costa, L. O. O.; Assaf, J. M.; Jacobs, G.; Davis, B. H.; Mattos, L. V.; Noronha, F. B. *Appl. Catal., A* **2010**, *377*, 181−190.
(23) Qiangshan, J.; Linxia, F.; Hui, L.; Xiaoming, Z. *J. Rare Earth* **2009**, *27*, 431−436.
(24) Zhao, B.; Wang, R.; Yang, X. *Catal. Commun.* **2009**, *10*, 1029−1033.
(25) Fierro, J. L. G. *Catal. Today* **1990**, *8*, 153−174.
(26) Liu, J. W.; Chen, G.; Li, Z. H.; An, W. W.; Zhang, Z. G. *J. Alloys Compd.* **2007**, *431*, 1−5.
(27) Nagabhushana, B. M.; Chakradhar, R. P. S.; Ramesh, K. P.; Prasad, V.; Shivakumara, C.; Chandrappa, G. T. *J. Alloys Compd.* **2008**, *450*, 364−368.
(28) Hong, W. J.; Iwamoto, S.; Inoue, M. *Catal. Today* **2011**, *164*, 489−492.
(29) Moradi, G. R.; Rahmanzadeh, M. *Catal. Commun.* **2012**, *26*, 169−172.
(30) Wei, J.; Iglesia, E. *Phys. Chem. Chem. Phys.* **2004**, *6*, 3754−3759.
(31) Xiaoping, D.; Changchun, Y.; Ranjia, L.; Qiong, W.; Kaijiao, S.; Zhengping, H. *J. Rare Earth* **2008**, *26*, 341−346.
(32) Pereñíguez, R.; González-DelaCruz, V.; Holgado, J.; Caballero, A. *Appl. Catal., B* **2010**, *93*, 346−352.
(33) Ferri, D.; Forni, L. *Appl. Catal., B* **1998**, *16*, 119−126.
(34) Wei, J. M.; Xu, B. Q.; Li, J. L.; Cheng, Z. X.; Zhu, Q. M. *Appl. Catal., A* **2000**, *196*, L167−L172.